Peer-reviewed version available at *Symmetry* **2018**, *10*, 604; doi:10.3390/sym10110604

Article

A Symmetry Motivated Link Table

Shawn Witte[1], Michelle Flanner[2] and Mariel Vazquez[1,2]

[1] UC Davis Mathematics
[2] UC Davis Microbiology and Molecular Genetics
* Correspondence: mrlvazquez@ucdavis.edu

Abstract: Proper identification of oriented knots and 2-component links requires a precise link nomenclature. Motivated by questions arising in DNA topology, this study aims to produce a nomenclature unambiguous with respect to link symmetries. For knots, this involves distinguishing a knot type from its mirror image. In the case of 2-component links, there are up to sixteen possible symmetry types for each topology. The study revisits the methods previously used to disambiguate chiral knots and extends them to oriented 2-component links with up to nine crossings. Monte Carlo simulations are used to report on writhe, a geometric indicator of chirality. There are ninety-two prime 2-component links with up to nine crossings. Guided by geometrical data, linking number and the symmetry groups of 2-component links, a canonical link diagram for each link type is proposed. All diagrams but six were unambiguously chosen ($8_1^2 5$, 9_5^2, $9_3^2 4$, $9_3^2 5$, $9_3^2 9$, and $9_4^2 1$). We include complete tables for prime knots with up to ten crossings and prime links with up to nine crossings. We also prove a result on the behavior of the writhe under local lattice moves.

Keywords: writhe; chirality; nomenclature; link symmetries; link table; knot table; lattice polygons; DNA topology

1. Introduction

The primary goal in the study of knot theory is to distinguish mathematical links. In the traditional link table in Rolfsen's *Knots and Links* each link diagram represents a link, its mirror, all orientations, and all component labelings [1]. Links differing in one or more of these ways may not be ambient isotopic. It is therefore often important to distinguish between two links which are related by reflections, orientation reversals, or component relabeling. For example, a chiral link is not topologically equivalent to its mirror image, an oriented link may not be equivalent to itself after reversing the orientation of a component, and different labelings of link components may not be equivalent. The objective of this study is to provide a link table that accounts for all of this information.

Our goal is to systematically define a set of canonical oriented links with labeled components so that any future research necessitating a distinction between link symmetries may refer to it and describe links via the naming convention and table of diagrams included here. We propose a method to choose the canonical link diagrams based on features which can be used to distinguish them from the other isotopy classes (section 4). These methods use linking number and numerical writhe data obtained from BFACF simulations (sections 6, 5), and they may be extended to links not included in this paper.

The work done in this paper extends the work of *Brasher et al.* and *Portillo et al.* [2,3]. In particular, we use self-avoiding polygons in $\mathbb{Z}^3$ to represent knots or link components, and we use BFACF simulations to examine the writhe behavior of links. *Portillo et al.* conjectured that given a knot K, there is a bounded interval (a, b) such that for every n, the mean of the writhes of all length n conformations

Preprints (www.preprints.org) | NOT PEER-REVIEWED | Posted: 15 August 2018 doi:10.20944/preprints201808.0265.v1

Peer-reviewed version available at Symmetry 2018, 10, 604; doi:10.3390/sym10110604

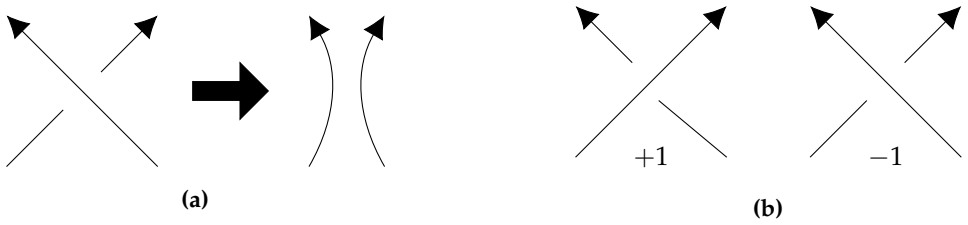

Figure 1. (a) Example of result DNA recombination modeled as coherent band surgery. **(b)** Contribution of one crossing to the projected writhe calculation.

of K in $\mathbb{Z}^3$ is in (a, b), and moreover, if K is chiral, then (a, b) does not contain 0, i.e. the entire interval is either positive or negative and the sign of the mean writhe is a knot invariant [2]. We extend this conjecture to links:

Conjecture 1. *Given a c-component link L, there are bounded intervals (a_i, b_i), for $1 \leq i \leq c$ such that the mean of the self-writhe of component i over length n conformations of L in $\mathbb{Z}^3$ falls within (a_i, b_i) for all n. Moreover, if the link is chiral, then either $\sum_i a_i < \sum_i b_i < 0$ for all n, or $0 < \sum_i a_i < \sum_i b_i$ for all n.*

Additionally, we had conjectured that if the link lacks exchange symmetry between component i and component j, then either $b_i < a_j$ for all n or $b_j < a_i$ for all n. We have found that this trend appears to be true for large n. We found, however, that for smaller values of n, this ordering may not be consistent. Specifically, minimum length conformations of the 8_{15}^2 link are provided as a counterexample (section 5).

We start in section 2 by defining writhe and linking number, which we will use to help distinguish the symmetry classes. Link symmetries and existing nomenclature are detailed and extended in section 3. We describe a systematic way to define a canonical isotopy class for each link (table A1) in section 4. The methods used to obtain the estimates required to classify link isotopies are presented in section 6. In section 5 we discuss the results of these simulations, and how they relate to conjecture 1, as well as provide a theorem which hints at the boundedness of writhe throughout lattice links of the same isotopy class. The sum of our work is represented in the selection of link diagrams presented in table A1 to be used as canonical oriented links with labeled components. In the supplementary materials, we also provide a writhe-based knot table (table S6) extended to 10 crossings based on the work of *Portillo et al.* and *Brasher et al.* [2,3].

Importance of Link Symmetries in DNA Topology

The motivation for this study comes from the need to unambiguously identify knots and links arising from biological processes that change the topology of DNA. In its most commons form, the B form, DNA forms a right handed double helix consisting of two sugar phosphate backbones held together by hydrogen bonds. The backbones have an inherent antiparallel chemical orientation ($5'$ to $3'$) and a circular molecule could be modeled as an orientable 2-component link where each backbone is represented by one component. More often, in DNA topology studies, the molecule is modeled as the curve drawn by the axis of the double helix. The axis can inherit the orientation of one of the backbones or be assigned an orientation based on its nucleotide sequence. In this way, one circular DNA molecule is modeled as an oriented knot. Different cellular processes can alter the topology of DNA. For example, DNA replication of one circular DNA molecule gives rise to a 2-component DNA link. The orientation given to the DNA circle before replication is naturally inherited by the components of the newly replicated link. Replication links are typically unlinked by enzymes in the family of type II topoisomerases which simplify the topology of their substrate DNA by a sequence of crossing changes. In [4], Grainge *et al.* showed that in *Escherichia coli*, in the absense of the topoisomerase Topo IV, replication links could be unlinked by site-specific recombination. Site-specific recombinases act by

Preprints (www.preprints.org) | NOT PEER-REVIEWED | Posted: 15 August 2018 doi:10.20944/preprints201808.0265.v1

Peer-reviewed version available at Symmetry 2018, 10, 604; doi:10.3390/sym10110604

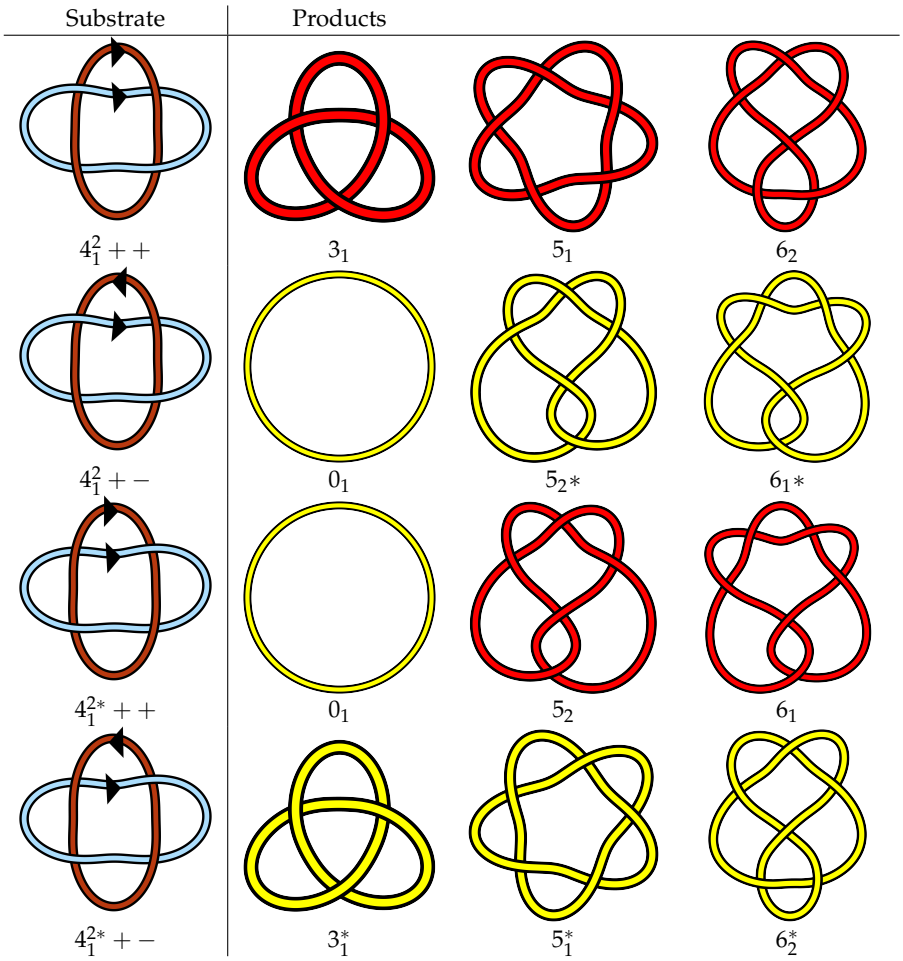

Figure 2. Isotopy types of the link 4_1^2 are pictured in the first column. Each row denotes a different isotopy type of the 4_1^2 used as the starting point for a coherent band surgery (local reconnection). These can be interpreted as substrates of site-specific recombination at two *dif* sites, one on each component of the link. The right side shows all the potential products of said event, up to crossing number 6, depending on the isotopy type of the substrate. It is clear in this example that coherent band surgery on the different isotopy types of the link 4_1^2 yield different knots. In particular 4_1^2+- and $4_1^{2*}++$ can be unknotted in one step, while 4_1^2++ and $4_1^{2*}+-$ cannot.

local reconnection, which can be modeled as a coherent band surgery on the substrate link (see figure 1a). This process was studied in [5,6]. Importantly, the outcome of recombination can be dependent on the exact symmetry class of the link being acted on (see figure 2).

Links arising as products of enzymatic reactions on circular substrates may have distinguishable components if the nucleotide sequence differs from one component to the other. Additionally, some enzymes in the group of topoisomerases and site-specific recombinases have been found to have a chirality bias when identifying their targets (topological selectivity) or to tie knots or links of particular topology and symmetry type (topological specificity). Complete distinction between links related by reflection, orientation changes, and component relabeling is important in many problems in physics and biology. For example, knots and links appear in the study of circular DNA molecules such as bacterial chromosomes as explained below.

2. Writhe and Linking Number

Linking number is a standard topological invariant of oriented links which may be calculated from a spatial conformation or a regular diagram. To calculate linking number of a link L from a

Peer-reviewed version available at Symmetry 2018, 10, 604; doi:10.3390/sym10110604

regular diagram of an oriented link, number the inter-component crossings from 1 to m, and assign characteristic ϵ_i to crossing i, where ϵ_i is either $+1$ or -1 according to the convention in figure 1b, then the linking number is $\mathrm{lk}(L) = \frac{1}{2}\sum_{i=1}^{m} \epsilon_m$. For a 2-component link embedded in space parametrized by curves $\gamma_1, \gamma_2 \colon \mathbb{S}^1 \to \mathbb{S}^3$, the linking number is calculated by the Gaussian integral

$$\mathrm{lk}(L) = \frac{1}{4\pi} \int_{\gamma_1} \int_{\gamma_2} \frac{(dr_2 \times dr_1) \cdot (r_2 - r_1)}{|r_2 - r_1|^3}, \tag{1}$$

where r_i are the vectors representing points along the curve γ_i [7].

Space writhe is a geometric invariant of a link conformation that measures entanglement complexity. The *space writhe* of a knot conformation σ parametrized by $\gamma \colon \mathbb{S}^1 \to \mathbb{S}^3$ is found by taking the integral

$$w(\sigma) = \frac{1}{4\pi} \int_{\gamma} \int_{\gamma} \frac{(dr_2 \times dr_1) \cdot (r_2 - r_1)}{|r_2 - r_1|^3}, \tag{2}$$

where r_i are the vectors representing points along the curve γ [7]. Note that space writhe is not a topological invariant.

For links with c components, each component has its own *self-writhe* calculated as above. We denote self-writhe of component i by $s(\sigma_i)$ where σ_i is the conformation of the ith component. The *sum of self-writhes* of a c-component link conformation $\sigma = \sqcup_{i=1}^{c} \sigma_i$ is $s(\sigma) = \sum_{i=1}^{c} s(\sigma_i)$. We define the *total writhe* of a link conformation σ as $w(\sigma) = s(\sigma) + 2lk(\sigma)$. Note that for a link L with conformation σ, we can write $\mathrm{lk}(\sigma) = \mathrm{lk}(L)$ since linking number is an invariant. However, this substitution cannot be made for $s(\sigma)$, as writhe is not a topological invariant.

3. Link Symmetries and Nomenclature

In this section, we define the different types of link symmetries and introduce the proposed link nomenclature.

3.1. Isotopy Classes

Two links are *equivalent* if there is an isotopy that transforms one into the other. The set of all conformations which are isotopically equivalent form an *isotopy class*. When a link L is not equivalent to its mirror image L*, then L and L* form two distinct isotopy classes. However, when link diagrams are listed in a table, only one of these two isotopy classes is represented. One may always infer the mirror image L* from the diagram of L. Specifically, the mirror image of a diagram is obtained by changing all over-crossings to under-crossings and vice versa. The number of potential isotopy classes is increased by assigning orientations and labeling components. For an oriented c-component link with labeled components, there are up to $2 \cdot 2^c \cdot c!$ distinct isotopy classes. This number comes from the 2 reflections, 2^c orientations, and $c!$ labelings of the components.

The symmetries of a c-component link can be described by a subgroup of $\Gamma_c = \mathbb{Z}_2 \times (\mathbb{Z}_2^c \rtimes S_c)$ [8]. The generator from the first $\mathbb{Z}_2$ represents reflection. The generator of the ith copy of $\mathbb{Z}_2$ in $\mathbb{Z}_2^c$ represents reversal of the ith component. A permutation $\alpha \in S_c$ represents a relabeling where component i is relabeled as $\alpha(i)$.

In this paper, we consider the cases where $c = 1, 2$, but strive to develop methods which can be generalized to $c \in \mathbb{N}$. When $c = 1$, there are two possible unoriented isotopy classes (the knot and its mirror image), and four possible oriented isotopy classes. For 2-component links, there are 16 possible isotopy classes for each oriented link with labeled components.

3.2. Doll and Hoste Notation

We use the notation of *Doll and Hoste* to differentiate isotopy classes of the same link type [9]. Consider an oriented 2-component link of link type L with labeled components. We will refer to this initial link as L++. If we have a link in which the ith component is reversed from L++, then we

Table 1. Symmetry groups for two-component links with up to 9 crossings. Listed are names for the groups and their notation as a subgroup of Γ_2 [8,10]. Also listed are generators for the subgroup where ϵ is a reflection, r_1 and r_2 are reversals of components 1 and 2, respectively, and p is the exchange of the component labels. The final column contains sets for which of the 16 different possible isotopy classes are equivalent to $L{+}{+}$ where τ is the non-trivial element of S_2.

Symmetry Name	Occurences for $c(L) \leq 9$	Subgroup of Γ_2	Generators of Subgroup	Equivalence Class of $L{+}{+}$
Full Symmetry	1	Γ_2	$\langle \epsilon, r_1, r_2, p \rangle$	$\{L{+}{+}, L{+}{-}, L{-}{+}, L{-}{-}, L^*{+}{+}, L^*{+}{-}, L^*{-}{+}, L^*{-}{-}, \tau L{+}{+}, \tau L{+}{-}, \tau L{-}{+}, \tau L{-}{-}, \tau L^*{+}{+}, \tau L^*{+}{-}, \tau L^*{-}{+}, \tau L^*{-}{-}\}$
Purely Inv. (Pure Ex.)	25	$\Sigma_{4,1}$	$\langle r_1 r_2, p \rangle$	$\{L{+}{+}, L{-}{-}, \tau L{+}{+}, \tau L{-}{-}\}$
Purely Inv. (No Ex.)	32	$\Sigma_{2,1}$	$\langle r_1 r_2 \rangle$	$\{L{+}{+}, L{-}{-}\}$
Fully Inv. (Pure Ex.)	5	$\Sigma_{8,1}$	$\langle r_1, r_2, p \rangle$	$\{L{+}{+}, L{+}{-}, L{-}{+}, L{-}{-}, \tau L{+}{+}, \tau L{+}{-}, \tau L{-}{+}, \tau L{-}{-}\}$
Fully Inv. (no Ex.)	22	$\Sigma_{4,2}$	$\langle r_1, r_2 \rangle$	$\{L{+}{+}, L{+}{-}, L{-}{+}, L{-}{-}\}$
Even Op. (Pure Ex.)	3	$\Sigma_{8,2}$	$\langle \epsilon r_1, \epsilon r_2, p \rangle$	$\{L{+}{+}, L{-}{-}, L^*{+}{-}, L^*{-}{+}, \tau L{+}{+}, \tau L{-}{-}, \tau L^*{+}{-}, \tau L^*{-}{+}\}$
Even Op. (Non-Pure Ex.)	1	$\Sigma_{4,5}$	$\langle \epsilon r_1 p, \epsilon r_2 p \rangle$	$\{L{+}{+}, L{-}{-}, \tau L^*{+}{-}, \tau L^*{-}{+}\}$
No Symmetry	3	$\{e\}$	$\langle e \rangle$	$\{L{+}{+}\}$

replace the ith $+$ with a $-$. If an oriented link is fully invertible (see below), the $+$'s and $-$'s may be omitted. The mirror image of L$+$$+$ is denoted by L*$+$$+$. Likewise the mirror images of L$+$$-$, L$-$$+$, and L$-$$-$ are L*$+$$-$, L*$-$$+$, and L*$-$$-$, respectively. This notation extends to c-component links by appending another $+$ or $-$ for each additional component. Note that this notation intrinsically assumes the components are labeled numerically from 1 to c.

We propose extending this notation by using an element of the permutation group, S_c, to denote other possible labelings given L$+\cdots+$. Let $\alpha \in S_c$, then we use the notation αL$+\cdots+$, to denote L$+\cdots+$ with the ith component relabeled to $\alpha(i)$ for each i. If α is the identity, then it may be omitted. Note that for 2-component links, α may only be the identity or the permutation exchanging 1 and 2. Applying this notation with reversals leaves an ambiguity for what order the relabeling and component reversals happen. For example, if L is a 2-component link and τ is the transposition of 1 and 2, then which component is reversed in τL$+$$-$? We take the convention that α is applied to L$\pm\cdots\pm$ after the orientations are determined. This means that the diagrams of L$+$$-$ and τL$+$$-$ will look identical except for the names assigned to the components. Which is to say L$+$$-$ and τL$+$$-$ have the same underlying unlabeled oriented link L$+$$-$. Figure 3 illustrates this notation in full for the 4_1^2 link.

3.3. Link Symmetries

Let Γ_2 be the full symmetry group for 2-component links. The subgroups of Γ_2 are enumerated and discussed by *Cantarella et al.* [10]. In particular there are 27 subgroups up to conjugacy. The jth order k subgroup of Γ_2 is designated $\Sigma_{k,j}$ [10]. When cross-referenced with the work of *Berglund et al.* and *Henry & Weeks*, we found that only 8 of the 27 subgroups occur for 2-component links with crossing number 9 or less [8,11]. Details of each of these subgroups are included in table 1. The symmetry names used come from the work of *Berglund et al.* and are defined as follows for a 2-component link L [8]:

- L is *purely invertible* if it is isotopic to the link found by simultaneously reversing both components ($L{+}{+}$=$L{-}{-}$).
- L is *fully invertible* if it is isotopic to L with every other choice of orientation.
- L has *even operations* symmetry if it is isotopic to links obtained by an even number of reflections and/or component reversals.

Peer-reviewed version available at Symmetry 2018, 10, 604; doi:10.3390/sym10110604

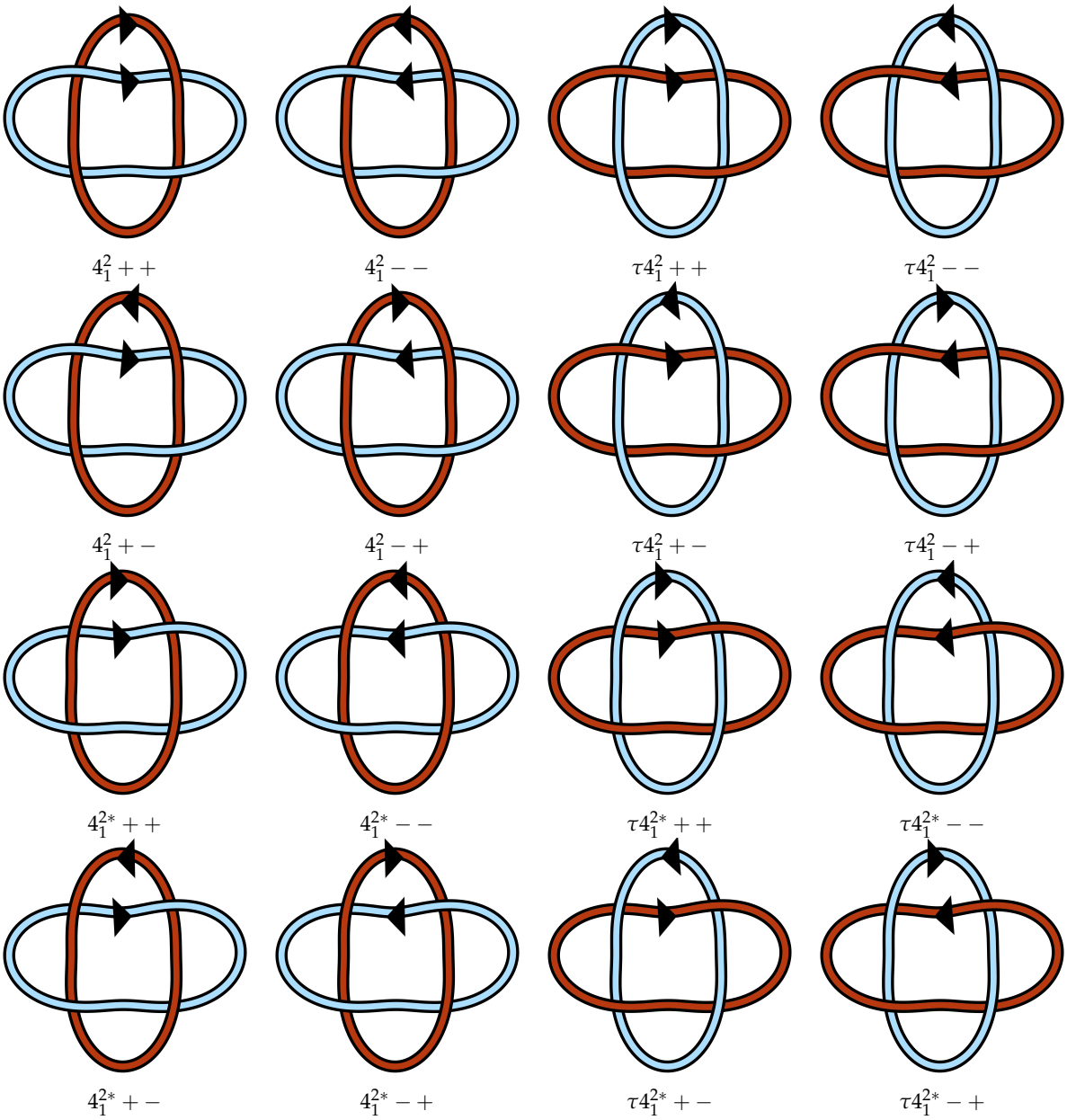

Figure 3. Example of the link notation adopted and modified from the work of *Doll and Hoste* [9]. The lighter blue strand is component 1 and the darker red-orange strand is component 2. Here, τ is the nontrivial element of S_2. Because 4_1^2 has symmetry group $\Sigma_{4,1}$, all links sharing a row in this figure are equivalent. The diagram labeled $4_1^2{+}{+}$ here matches the diagram in table A1. All other diagrams are determined from $4_1^2{+}{+}$.

- L has *pure exchange* symmetry if it is isotopic to L with the component labels exchanged ($L{+}{+}{=}\tau L{+}{+}$).
- L has a *non-pure exchange* symmetry if it is isotopic to L with a combination of exchanged labels with a reflection and/or component reversals, but $L{+}{+}{\neq}\tau L{+}{+}$.
- L has *no exchange* symmetry, if it is not isotopic to L with the component labels exchanged regardless of any reversals or reflections.
- L has *full symmetry* if it is isotopic to every link obtained by component relabeling, component reversal, and reflection.
- L has *no symmetry* if it is not isotopic to any link obtained by component relabeling, component reversal, or reflection.

It is interesting to note that of the 8 symmetry types observed for prime 2-component links with no more than 9 crossings, only links with no symmetry lack any kind of inversion symmetry. More specifically, every prime 2-component link with at most 9 crossings has L++= L−− except for the 9^2_{34}, 9^2_{35}, and 9^2_{39} links which each have no symmetry. Also, the only links which have any kind of reflection symmetry are those with even operations symmetry or full symmetry. There are only four prime 2-component links with crossing number 9 or less that have even operations symmetry, and the only observed 2-component link with full symmetry is 0^2_1 [10]. All other prime 2-component links lack reflection symmetry.

For the purposes of classification of isotopy types, the more interesting links are those which lack certain symmetries, as there will be more isotopy classes to disambiguate. As we will see in section 3.4, writhe is connected to the isotopy class of links which lack pure exchange and/or reflection symmetries. Because of this, those links will be of particular interest to the results of our writhe experiments described in section 6. Of the 92 prime 2-component links with crossing number 9 or less, 58 lack pure exchange symmetry and 87 lack reflection symmetry.

3.4. Symmetries and Writhe/Linking Number

Consider a 2-component link L++ with linking number $\mathrm{lk}(\mathrm{L}++) \neq 0$. A link diagram for the mirror image, L^*++, can be obtained by taking a diagram for L++ and switching all of the over/under-crossings. This changes the sign of each crossing's contribution to the linking number, hence $\mathrm{lk}(\mathrm{L}++) = -\mathrm{lk}(\mathrm{L}^*++)$. So an oriented link with non-zero linking number cannot be equivalent to its mirror image as an oriented link. Note that it could, for example, have even operations symmetry which would make it equivalent to its mirror as an unoriented link.

Similarly, reversing the orientation of one of the components will change the characteristic of each inter-component crossing, i.e.

$$\mathrm{lk}(L++) = \mathrm{lk}(L--) = -\mathrm{lk}(L-+) = -\mathrm{lk}(L+-) \tag{3}$$

Thus, linking number can help discern choices of orientation. Note that reversing the orientation of a link component does not change self-writhe of that component.

Taking the mirror image of a link will yield the opposite self-writhes, linking number, and total space writhe, i.e. for a c-component link L in conformation σ with components σ_i,

$$s(\sigma_i) = -s(\sigma_i^*),\ s(\sigma) = -s(\sigma^*),\ \mathrm{lk}(\sigma) = -\mathrm{lk}(\sigma^*), \text{ and } w(\sigma) = -w(\sigma^*) \tag{4}$$

where σ^* is the reflection of conformation σ. We observe that writhe is in some way dependent on chirality, but not orientation, whereas linking number is dependent on both.

3.5. Previous Classification Schemes

There have been previous attempts to classify link isotopy classes. For chirality, *Liang et al.* classified alternating links into chiral designations of either D or L based on a method called *writhe profiles* which is related to projected writhes [12]. While writhe profiles provide a useful way to classify many alternating knots and links, they do not classify non-alternating knots and links. Moreover, there is a discrepancy in the work of *Liang et al.* between how oriented and non-oriented links are classified, as explained below.

For non-oriented links, the sign of the projected writhe is checked and the link is assigned a D for a positive value and an L for a negative value. If the sum of self-writhes is zero, writhe profiles are calculated in order to specify a designation of D or L.

For oriented links, the sign of the linking number is checked first and the link is assigned a D for a positive value and an L for a negative value. If linking number is zero, the designation process for the non-oriented links is followed, with minor changes to account for orientation.

A discrepancy arises when linking number is non-zero. Chirality is a property independent of orientation. However linking number very much depends on orientation. Thus, linking number is not a good choice for a chiral designator. To see the issue more clearly, take the link 4_1^2 as an example. The 4_1^2 link has 4 oriented symmetry classes which can be represented by $4_1^2{+}{+}$, $4_1^2{+}{-}$, $4_1^{2*}{+}{+}$, and $4_1^{2*}{+}{-}$ (see figure 3). However, it only has 2 unoriented symmetry classes which could be represented by 4_1^2 and 4_1^{2*}. In the classification of *Liang et al.*, the link designated $4_1^2{+}{+}$ in figure 3 would be given a D classification, while $4_1^2{+}{-}$ gets classified with an L [12]. However, since $4_1^2{+}{+}$ and $4_1^2{+}{-}$ both share the same underlying unoriented link, 4_1^2, they should be given the same chiral designation, as chirality is a property the unoriented link.

Our classification method (section 4) will also use writhe, but only to distinguish and classify link mirrors and component labelings. We will also use linking number, but only to distinguish orientations.

4. Defining a Canonical Isotopy Class for Links

In order to classify link isotopy classes, we will use Monte Carlo sampling of writhe. This sampling is performed via the BFACF algorithm, which applies to cubic lattice links.

4.1. Cubic Lattice Links and the BFACF Algorithm

The numerical methods of this paper use links in the cubic lattice, $\mathbb{Z}^3$. We will refer to these as *lattice links*. A c-component lattice link is a disjoint union of c self-avoiding polygons. A *self-avoiding polygon* of length n is a sequence of points $\{v_1, v_2, ..., v_n\}$ in $\mathbb{Z}^3$ such that $|v_i - v_{i+1}| = 1$ for $i = 1, 2, 3, ..., n-1$, $|v_n - v_1| = 1$, and $v_i \neq v_j$ for all $i \neq j$. To obtain the polygon from these points, we include the edges e_i, $i = 1, .., n$ where e_i is the edge connecting v_i and v_{i+1}, with e_n connecting v_n and v_1. The *length of a link in* $\mathbb{Z}^3$ is the sum of the lengths of the components of the link. We will denote the length of a lattice link σ by $|\sigma|$.

This representation is advantageous as it allows us to use the BFACF algorithm to sample a distribution of link conformations and analyze geometric trends such as writhe. The BFACF algorithm is a dynamic Markov chain Monte Carlo algorithm with a state space of self-avoiding walks in $\mathbb{Z}^3$ [13–15]. In our case, the state spaces will specifically be lattice link isotopy classes. Transitions in the chain are deformations of the link as seen in figure 4a. It has been shown that the ergodicity class of a knot or link in BFACF is the set of all possible embeddings within that knot or link's isotopy class in $\mathbb{Z}^3$ [16].

The transition probabilities of BFACF depend on a parameter $z \in (0, z_0)$ where $z_0 \approx 0.2134$ [16]. The limiting distribution of this Markov chain is

$$\pi(\sigma) = \frac{|\sigma| z^{|\sigma|}}{\Xi(z)} \tag{5}$$

where

$$\Xi(z) = \sum_{n=4}^{\infty} n_z^n \mu_n(L), \tag{6}$$

and $\mu_n(L)$ is the total number of length n lattice links in the same isotopy class as L. This distribution has the property that all conformations of the same length have equal probability, dependent only on z and the link type. Thus, the BFACF algorithm may be used to uniformly sample conformations of certain link isotopy class and length. The reader is directed to [17, chapter 9] for a full treatment of the BFACF algorithm.

4.2. Canonical Isotopy Class

When one refers to a link, most commonly they use the name listed in the Rolfsen table [1]. This is effective for communicating links, but when working with oriented links or links with distinguished

Preprints (www.preprints.org) | NOT PEER-REVIEWED | Posted: 15 August 2018 doi:10.20944/preprints201808.0265.v1

Peer-reviewed version available at Symmetry 2018, 10, 604; doi:10.3390/sym10110604

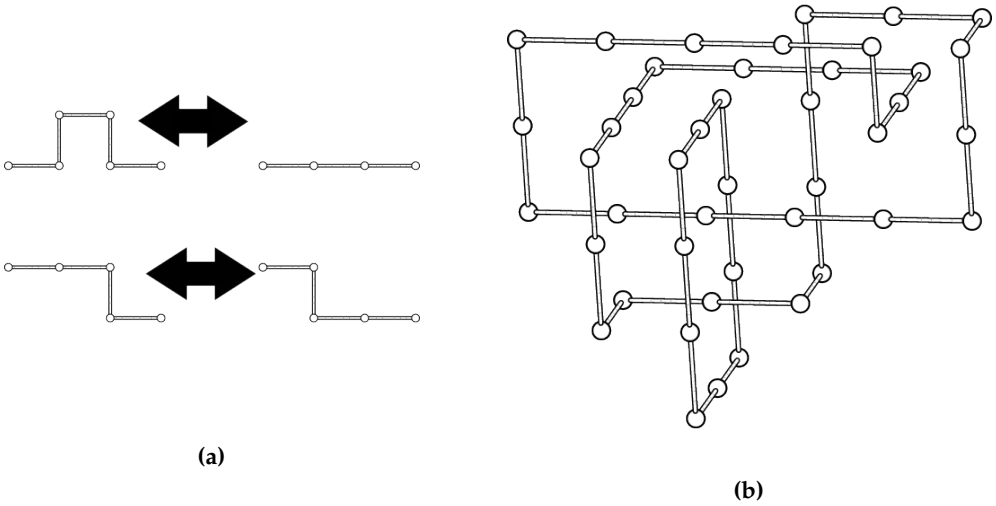

(a) **(b)**

Figure 4. (a) BFACF moves: (±2)-move, top; (+0)-move, bottom. **(b)** A minimum step cubic lattice representation of the 8_{15}^2 link.

components, one must still explicitly draw a picture of the link for full clarity. *Doll & Hoste* provided a link table which included orientation and component labels in addition to providing a nomenclature for reversing components [9]. While the diagrams in the *Doll & Hoste* table were chosen in a systematic way (using Conway notation), there is inconsistency in which isotopy classes of each link are actually represented. For example, the two diagrams listed for 7_3^2 are reflections of each other and are non-isotopic, since 7_3^2 lacks reflection symmetry.

Our goal is to propose a systematic way to identify a representative isotopy class for each link type. We use writhe and linking number to aid in this. Let $\mathcal{C}_n(L)$ be the set of all length n lattice conformations of L. Let the average of the sum of self-writhes of the elements of $\mathcal{C}_n(L)$ be $\mathcal{S}_n(L)$, i.e.

$$\mathcal{S}_n(L) = \frac{1}{|\mathcal{C}_n(L)|} \sum_{\sigma \in \mathcal{C}_n(L)} s(\sigma). \tag{7}$$

Analogously, let σ_i be the self-avoiding polygon representing the ith component of $\sigma \in \mathcal{C}_n(L)$, then we define the average of the self-writhes of component i of L as

$$\mathcal{S}_n(L,i) = \frac{1}{|\mathcal{C}_n(L)|} \sum_{\sigma \in \mathcal{C}_n(L)} s(\sigma_i). \tag{8}$$

Case 1, L is a knot ($c = 1$)

In the case of knots, we follow the writhe-guided nomenclature proposed in *Portillo et al.* and *Brasher et al.* [2,3]. This nomenclature said that the canonical knot K was the one where $\mathcal{S}_n(K) > 0$. They also showed that for each chiral knot K, $\mathcal{S}_n(K)$ was either consistently positive or consistently negative regardless of n, hence this is an unambiguous designation. Using the data from those papers and previously unpublished 10-crossing data, we constructed a table of knots through 10-crossings (table S6). Note that these knots do not include orientation information, as the methods used do not discern orientations of knots.

Case 2, L is a 2-component link ($c = 2$)

The case of 2-component links is more complicated due to the extra link symmetries as detailed in section 3 and table 1. We appeal to conjecture 1 and use self-writhes and linking number to define the canonical isotopy class of a link, and denote it by L++. In particular, we choose L++ so that

$\mathcal{S}_n(\mathrm{L}{+}{+}) > 0$, $\mathrm{lk}(\mathrm{L}{+}{+}) > 0$, and $\mathcal{S}_n(L,1) > \mathcal{S}_n(L,2)$ when possible. Once L++ is chosen, it can be used as a point of reference for obtaining all other isotopy classes of the link as described in section 3.2, and seen in figure 3.

As long as $\mathcal{S}_n(\mathrm{L}{+}{+}) \neq 0$, then half of the isotopy classes will have $\mathcal{S}_n(\mathrm{L}{+}{+}) > 0$. Then, if $\mathrm{lk}(\mathrm{L}{+}{+}) \neq 0$, half of those isotopy classes will have $\mathrm{lk}(\mathrm{L}{+}{+}) > 0$. Then, as long as $\mathcal{S}_n(L,1) \neq \mathcal{S}_n(L,2)$, half of those isotopy classes will have $\mathcal{S}_n(L,1) > \mathcal{S}_n(L,2)$. This narrows down the 16 isotopy classes to two potential candidates for L++. If L has pure exchange symmetry, then these candidates are equivalent and the canonical link L++ is chosen to be this isotopy class. There are three 2-component links with crossing number at most 9 that lack pure exchange symmetry, namely 9^2_{34}, 9^2_{35}, and 9^2_{39} which each have no symmetry.

The assumptions that $\mathcal{S}_n(\mathrm{L}{+}{+}) \neq 0$, $\mathrm{lk}(\mathrm{L}{+}{+}) \neq 0$, and $\mathcal{S}_n(L,1) \neq \mathcal{S}_n(L,2)$ depend on the symmetry type of L. If there is reflection symmetry, then it is necessarily true that $\mathcal{S}_n(\mathrm{L}{+}{+}) = 0$ for all n. If $\mathcal{S}_n(\mathrm{L}{+}{+}) = 0$ and there is no reflection symmetry, then we cannot distinguish the link from its mirror image with our methods, but we did not observe this behavior. If there is pure exchange symmetry, then it is necessarily true that $\mathcal{S}_n(L,1) = \mathcal{S}_n(L,2)$. If $\mathcal{S}_n(L,1) = \mathcal{S}_n(L,2)$ and there is no pure exchange symmetry, then we cannot distinguish the different component labelings with our methods, but we did not observe this behavior either. For links with full inversion symmetry, it is necessarily true that $\mathrm{lk}(\mathrm{L}{+}{+}) = 0$. If $\mathrm{lk}(\mathrm{L}{+}{+}) = 0$ and L does not have full inversion symmetry, then we cannot distinguish orientations with our methods. This behavior is observed for 9^2_5 and 9^2_{41}.

In section 6, we describe the methods used to estimate $\mathcal{S}_n(L)$, $\mathcal{S}_n(L,1)$, and $\mathcal{S}_n(L,2)$ for each 2-component link through 9 crossings. Section 5 describes results of the numerical simulations, and analytical result on the affect of BFACF moves on the writhe of a lattice polygon. Partial data are presented in table 2 and figure 6 with complete data presented in supplementary tables S2, S3, S4, and S5.

4.3. Proposed Link Table

The canonical isotopy class was chosen for each link as described in section 4.2 using data obtained as described in sections 5 and 6. The 9^2_5, 9^2_{34}, 9^2_{35}, 9^2_{39}, and 9^2_{41} links each had two potential candidates for a canonical link. We chose to include one of the candidates in the table for each of these links to keep the table complete, but omitted the other candidate to avoid the ambiguities of nomenclature that we are attempting to eliminate. For each of these problematic links, some future analysis might find that our L−− is a better choice for the canonical isotopy class. The chosen canonical link diagrams are represented in table A1.

4.4. Note on minimum lattice links

In *Portillo et al.* an ideal lattice knot of type K was defined as a minimal step number (msn) lattice embedding of K[2]. The authors conjectured that the mean writhe of random polygons of given knot type and fixed length could be approximated by the mean writhe of the corresponding ideal msn conformation. They provided numerical evidence that there exists a constant α_K such that the mean writhe of a random lattice polygon of type K and length n belongs to $(w_I(K) - \alpha_K, w_I(K) + \alpha_K)$, independently of the value of n, where $w_I(K)$ is the mean writhe of the ideal lattice conformations of K. We here inquire if this conjecture can be extended to links. Methods and results are presented in sections 5 and 6.

5. Results and Discussion

5.1. Numerical Results

Statistically independent ensembles of linked lattice polygons were obtained as described in sections 4.1 and 6. We calculated $s(\sigma)$, $s(\sigma_1)$, and $s(\sigma_2)$ for each sampled conformation σ. Using batch mean analysis to account for autocorrelation, these values were used to calculate 95% confidence

intervals for $\mathcal{S}_n(L)$, $\mathcal{S}_n(L,1)$, $\mathcal{S}_n(L,2)$ with $n \in \{76,100,150,200,250,300\}$. For each link without reflection symmetry, each confidence interval for $\mathcal{S}_n(L)$ was found to be either entirely positive or entirely negative. Moreover, the signs of these confidence intervals are consistent across all sampled lengths for each link as predicted by conjecture 1.

For links which lack pure exchange symmetry, confidence intervals for $\mathcal{S}_n(L,1)$ and $\mathcal{S}_n(L,2)$ are disjoint at each n. Moreover, we can choose a labeling of component 1 and component 2 for each link so that $\mathcal{S}_n(L,1) > \mathcal{S}_n(L,2)$ for $n \in \{76,100,150,200,250,300\}$. From this, we were able to choose canonical link isotopies as described in section 4. The data for $\mathcal{S}_n(L)$, $\mathcal{S}_n(L,1)$ and $\mathcal{S}_n(L,2)$ for links with up to nine crossings are presented in supplementary tables S2, S3, and S4.

A regular diagram for each canonical isotopy class can be found in table A1. All data presented in this paper has been converted from sampled isotopy classes to $L{+}{+}$ by relabeling components and negating writhe and linking number where appropriate. The confidence intervals of the mean writhes at $n = 200$ for links up to crossing number 8 are presented in table 2 while an extended table including 9-crossing information is included in supplementary materials (table S5). These tables also list the link isotopy class from Rolfsen's table and Knotplot using the notation from section 3.2 based on our canonical choice as $L{+}{+}$ [1,10,18].

When the estimated values of $\mathcal{S}_n(L)$ and $\mathcal{S}_m(L)$ are compared for $n,m \in \{76,100,150,200,250,300\}$, they are found to only vary by a small amount. For each link, L, and pair of lengths, n and m, we estimated $|\mathcal{S}_n(L) - \mathcal{S}_m(L)|$. The largest difference for $\mathcal{S}_n(L)$ was found in the 8_1^2 link, where $\mathcal{S}_{250}(L)$ is estimated to be about 2.411 compared to 2.589 for $\mathcal{S}_{76}(L)$ for a difference of about 0.178. Figure 6 illustrates this behavior of $\mathcal{S}_n(L)$.

For individual component self-writhe, the largest difference was in $\mathcal{S}_n(9_{40}^2,1)$, where $\mathcal{S}_{250}(9_{40}^2,1)$ was estimated at 2.439 compared to 2.211 for $\mathcal{S}_{76}(9_{40}^2,1)$, giving a difference of about 0.228. For comparison, writhe in $\mathbb{Z}^3$ is always a multiple of $1/4$, so no two links or link components can differ in writhe by less than 0.25 [19]. In this way, $\mathcal{S}_n(L)$ and $\mathcal{S}_n(L,i)$ appear to be well-behaved.

Table 2. Mean self-writhes of minimum step prime 2-component links with 8 or fewer crossings. Numbers based on all conformations found in the pending paper by *Freund et al.* [22]

Link	$\mathcal{S}_{\min}(L)$	$\mathcal{S}_{\min}(L,1)$	$\mathcal{S}_{\min}(L,2)$
0_1^2	0.0	0.0	0.0
2_1^2	0.0	0.0	0.0
4_1^2	0.8125	0.4063	0.4063
5_1^2	1.3492	0.6746	0.6746
6_1^2	1.65	0.825	0.825
6_2^2	0.0	0.0	0.0
6_3^2	1.9438	0.9719	0.9719
7_1^2	2.1636	1.0818	1.0818
7_2^2	0.7	0.35	0.35
7_3^2	2.4903	2.4427	0.0476
7_4^2	4.2553	4.1811	0.0743
7_5^2	2.3625	2.7563	−0.3937
7_6^2	1.4375	1.4375	0.0
7_7^2	3.5368	3.5368	0.0
7_8^2	3.0479	3.0479	0.0
8_1^2	2.597	1.2985	1.2985
8_2^2	0.8123	0.4062	0.4062
8_3^2	2.7172	1.3586	1.3586
8_4^2	0.8164	0.4082	0.4082
8_5^2	1.1765	0.5883	0.5883
8_6^2	3.1666	1.5833	1.5833
8_7^2	2.7215	1.3607	1.3607
8_8^2	0.0	0.0	0.0
8_9^2	0.9355	0.6021	0.3333
8_{10}^2	0.9525	0.7288	0.2236
8_{11}^2	4.6944	4.6667	0.0278
8_{12}^2	2.0538	2.2909	−0.237
8_{13}^2	2.1324	2.1324	0.0
8_{14}^2	3.0967	3.0967	0.0
8_{15}^2	0.2157	0.0	0.2157
8_{16}^2	0.5	0.5	0.0

We also analyzed minimum step links (described in section 6.2, table 3 and in the supplementary materials table S1) and found that $\mathcal{S}_{\min}(L)$ and $\mathcal{S}_{\min}(L,i)$ also stayed reasonably close to the other values of $\mathcal{S}_n(L)$ and $\mathcal{S}_n(L,i)$. We did, however, find $\mathcal{S}_{\min}(8_{15}^2{+}{+},1) = 0$ and $\mathcal{S}_{\min}(8_{15}^2{+}{+},2) \approx 0.2157$, while $\mathcal{S}_n(8_{15}^2,1) > \mathcal{S}_n(8_{15}^2,2)$ for all other sampled lengths, which shows that component self-writhe of minimum step conformations may not be a sufficient indicator of self-writhe as n increases. We examined the minimum step 8_{15}^2 conformations in our dataset and observed that component 1 was identical in all of them; it was planar rectangle which always has 0 writhe. One of the minimum step conformations for 8_{15}^2 can be found in figure 4b.

5.2. Boundedness of Writhe under BFACF moves

BFACF moves not only define our sampling method, but also function as Reidemeister moves for lattice links in the sense that any lattice link conformation can be transformed into any other lattice conformation of the same link by a finite sequence of BFACF moves [16]. It is of interest, then, how BFACF moves may affect space writhe. We find that not only do BFACF moves affect space writhe in a bounded way, but writhe changes in a way entirely predicted by the local geometry of the edges within two steps of the BFACF move. To prove this, we will appeal to a special formulation of space writhe for lattice links proven by *Lacher & Sumners* [20].

To perform the lattice link writhe calculation, we first define the *push-off* $\sigma_{(\varepsilon_1,\varepsilon_2,\varepsilon_3)}$ of a lattice link σ for $\varepsilon_i \in (-1,0)\cup(0,1)$. We obtain $\sigma_{(\varepsilon_1,\varepsilon_2,\varepsilon_3)}$ by translating σ along the vector $[\varepsilon_1,\varepsilon_2,\varepsilon_3]^T$.

Theorem 1 ([20]). *The total writhe of a lattice link may be calculated as follows:*

$$w(\sigma) = \frac{lk(\sigma,\sigma_{(\frac{1}{2},\frac{1}{2},\frac{1}{2})}) + lk(\sigma,\sigma_{(-\frac{1}{2},\frac{1}{2},\frac{1}{2})}) + lk(\sigma,\sigma_{(\frac{1}{2},\frac{1}{2},-\frac{1}{2})}) + lk(\sigma,\sigma_{(-\frac{1}{2},\frac{1}{2},-\frac{1}{2})})}{4} \tag{9}$$

where $lk(\sigma_i,\sigma_j)$ is the linking number of $\sigma_i \sqcup \sigma_j$.

Since we can calculate the total writhe of a link from the self-writhes of the individual components, equation (9) is sufficient to find writhe for links with any number of components. This yields the following interesting corollary:

Corollary 1 ([20]). *If σ is a simple cubic lattice representation of a link, then $w(\sigma) = \frac{k}{4}$ for some $k \in \mathbb{Z}$.*

A BFACF move is performed by taking an edge of a self-avoiding polygon in $\mathbb{Z}^3$ and pushing it one unit in one of the four directions perpendicular to the direction of the edge. We will refer to the edge being pushed as the *BFACF edge*. If an endpoint of the BFACF edge traces an existing edge of the polygon during that push, then the traced edge is deleted. On the other hand, if an endpoint of the BFACF edge does not trace another edge of the polygon, then an edge is added in the traced space. With this in mind, we prove the following theorem:

Theorem 2. *If σ_1 and σ_2 are related by a single BFACF move, then $|w(\sigma_2) - w(\sigma_1)| \leq \frac{1}{2}$. More specifically, $(w(\sigma_2) - w(\sigma_1)) \in \{-\frac{1}{2}, -\frac{1}{4}, 0, \frac{1}{4}, \frac{1}{2}\}$.*

Proof. We will consider the BFACF move which transforms σ_1 into σ_2. Without loss of generality, we may assume that

1. the BFACF edge runs from $(0,0,0)$ to $(0,1,0)$, and
2. the result of the BFACF move will push the BFACF edge to an edge from $(0,0,-1)$ to $(0,1,-1)$.

We make rotate and translate the conformation to make these assumptions true, which will not affect the writhe of the conformations.

Now consider the BFACF move. This move may pass the lattice through one of the push-offs from theorem 1, changing the linking number of the polygon with that push-off. One such strand passage will change the linking number by ± 1, in turn changing the space writhe by $\pm 1/4$. If the move passes the polygon through a push-off edge, then the push-off edge must have endpoints $(-1/2,1/2,-1/2)$ and $(1/2,1/2,-1/2)$ (e.g. the black BFACF edge and orange push-off edge in figure 5). Checking where this edge must come from in the original polygon by reversing the push-off, we see it is necessary that this edge either has an endpoint at $(0,0,0)$ or at $(0,0,-1)$. In the former case this means that the edge before to the BFACF edge runs in the x direction, and there are two such possible edges. In the latter case, the edge before the BFACF edge must run from $(0,0,-1)$ to $(0,0,0)$ and the edge before that must run in the x direction, and there are two such possible edges. If there is no edge from $(0,0,-1)$

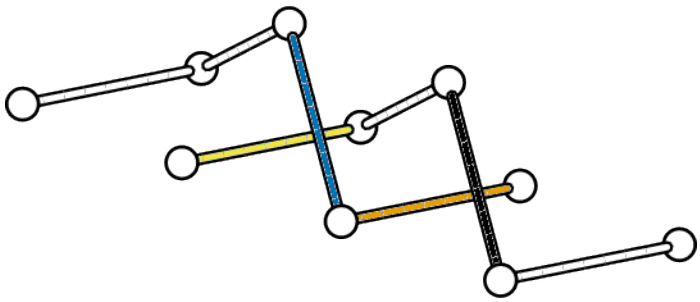

Figure 5. If a BFACF move is performed on the black edge in the direction of the orange (medium gray in grayscale) edge of the push-off beneath it, then the linking number with the push-off will change by -1 which will change the writhe by $-1/4$. This same BFACF move will also push the blue (dark gray) edge of the push-off through the yellow (light gray) edge of the link, which will cause the linking number to change by another -1, hence this will contribute a $-1/4$ change to the writhe. So, a BFACF move pushing the black edge into the page will result in a lattice link with a writhe $1/2$ less than the current link's writhe.

to $(0,0,0)$, then this second case will result in a self-intersection of the link and is not a valid BFACF move. We can see that the four possible edges to result in this change are all mutually exclusive, so from all of these cases, only one can contribute the $\pm 1/4$ change in writhe.

Now suppose that one of the push-offs of the BFACF edge passes through an edge of the original link when the BFACF move is performed (e.g. the blue push-off edge being pushed through the yellow edge in figure 5). The four push-offs of the BFACF edge run from $(-1/2,1/2,-1/2)$ to $(-1/2,3/2,-1/2)$, $(1/2,1/2,-1/2)$ to $(1/2,3/2,-1/2)$, $(-1/2,-1/2,-1/2)$ to $(-1/2,1/2,-1/2)$, and $(1/2,-1/2,-1/2)$ to $(1/2,1/2,-1/2)$. We note that in each of these cases the edge which the crossing change is occuring with must be running in the x direction and have an endpoint at either $(0,1,0)$ or $(0,1,-1)$. Similar to the previous cases, each of these possible edges are mutually exclusive and must either be the edge after the BFACF edge or the edge after that. Again, since they are mutually exclusive cases, the change in writhe from these cases can only be $\pm 1/4$.

So, at most two of the above cases may be true at any given time, each contributing to a change in writhe of $\pm 1/4$. So the total change in writhe from any BFACF move is in the set $\{-\frac{1}{2}, -\frac{1}{4}, 0, \frac{1}{4}, \frac{1}{2}\}$. □

Table 3. Columns 2,3, and 4 show confidence intervals for the average of the sum of self-writhes ($\mathcal{S}_{200}(L{+}{+})$), and self-writhes of components 1 and 2 ($\mathcal{S}_{200}(L{+}{+},1)$ and $\mathcal{S}_{200}(L{+}{+},2)$) for length 200 links in $\mathbb{Z}^3$. For each 2-component link indicated in column 1, the average is taken over an ensemble of statistically independent length 200 lattice links of type L as described in the numerical methods section. Combined with the linking number (column 7), these confidence intervals are used to determine which diagram appears as L++ in table A1. The Rolfsen ([1]) diagram's designation under our notation is presented in column 5. Column 6 lists which isotopy class is represented by default KnotPlot. Note that the KnotPlot conformations are reflections of the Rolfsen Table. Symmetry groups (column 8) are taken from the work of *Henry & Weeks*, *Berglund et al.*, and from SnapPy [8,11,21].

L	$\mathcal{S}_{200}(L)$	$\mathcal{S}_{200}(L,1)$	$\mathcal{S}_{200}(L,2)$	Rolfsen	KP	lk(L)	Sym
0_1^2	[− −]	[− −]	[− −]	0_1^2	$0_1^2{+}{+}$	0	Γ_2
2_1^2	[−0.037 0.102]	[−0.054 0.043]	[−0.106 0.087]	2_1^2	$2_1^2{+}{+}$	1	$\Sigma_{8,2}$
4_1^2	[0.755 0.877]	[0.391 0.481]	[0.336 0.424]	4_1^{2*}	$4_1^2{+}-$	2	$\Sigma_{4,1}$
5_1^2	[1.401 1.607]	[0.685 0.844]	[0.657 0.822]	5_1^{2*}	$5_1^2{+}{+}$	0	$\Sigma_{8,1}$
6_1^2	[1.624 1.692]	[0.812 0.862]	[0.795 0.847]	6_1^{2*}	$6_1^2{+}{+}$	3	$\Sigma_{4,1}$
6_2^2	[−0.156 0.042]	[−0.144 0.014]	[−0.067 0.083]	6_2^2	$6_2^2{+}{+}$	3	$\Sigma_{8,2}$
6_3^2	[1.957 2.225]	[0.979 1.207]	[0.892 1.105]	6_3^{2*}	$6_3^2{+}-$	2	$\Sigma_{4,1}$
7_1^2	[2.188 2.364]	[1.027 1.167]	[1.109 1.249]	7_1^{2*}	$7_1^2{+}{+}$	1	$\Sigma_{4,1}$
7_2^2	[0.413 0.788]	[0.211 0.509]	[0.093 0.389]	7_2^{2*}	$7_2^2{+}-$	1	$\Sigma_{4,1}$
7_3^2	[2.667 2.728]	[1.318 1.373]	[1.324 1.38]	7_3^{2*}	$7_3^2{+}{+}$	0	$\Sigma_{8,1}$
7_4^2	[4.292 4.348]	[3.992 4.04]	[0.289 0.319]	7_4^2	$7_4^{2*}{+}{+}$	0	$\Sigma_{4,2}$
7_5^2	[2.532 2.602]	[2.843 2.904]	[−0.326 − 0.286]	7_5^{2*}	$\tau 7_5^2{+}{+}$	2	$\Sigma_{2,1}$
7_6^2	[1.411 1.445]	[1.381 1.41]	[0.023 0.042]	7_6^{2*}	$\tau 7_6^2{+}{+}$	0	$\Sigma_{4,2}$
7_7^2	[3.51 3.592]	[3.458 3.527]	[0.036 0.081]	7_7^2	$7_7^{2*}{+}{+}$	2	$\Sigma_{2,1}$
7_8^2	[3.248 3.324]	[3.304 3.368]	[−0.07 − 0.03]	7_8^{2*}	$\tau 7_8^2{+}{+}$	0	$\Sigma_{4,2}$
8_1^2	[2.443 2.477]	[1.225 1.251]	[1.209 1.235]	8_1^{2*}	$8_1^2{+}-$	4	$\Sigma_{4,1}$
8_2^2	[0.761 0.79]	[0.373 0.396]	[0.379 0.403]	8_2^2	$8_2^{2*}{+}{+}$	4	$\Sigma_{4,1}$
8_3^2	[2.861 2.907]	[1.435 1.474]	[1.41 1.449]	8_3^{2*}	$8_3^2{+}{+}$	3	$\Sigma_{4,1}$
8_4^2	[0.868 0.94]	[0.417 0.476]	[0.429 0.486]	8_4^{2*}	$8_4^2{+}-$	4	$\Sigma_{4,1}$
8_5^2	[1.171 1.22]	[0.575 0.618]	[0.578 0.62]	8_5^{2*}	$8_5^2{+}{+}$	3	$\Sigma_{4,1}$
8_6^2	[3.29 3.33]	[1.632 1.671]	[1.639 1.678]	8_6^{2*}	$8_6^2{+}{+}$	2	$\Sigma_{4,1}$
8_7^2	[2.829 2.864]	[1.415 1.445]	[1.402 1.431]	8_7^{2*}	$8_7^2{+}-$	1	$\Sigma_{4,1}$
8_8^2	[−0.002 0.033]	[0.006 0.035]	[−0.02 0.01]	8_8^2	$8_8^2{+}{+}$	1	$\Sigma_{8,2}$
8_9^2	[0.777 0.92]	[0.471 0.599]	[0.276 0.35]	8_9^2	$\tau 8_9^{2*}{+}{+}$	2	$\Sigma_{2,1}$
8_{10}^2	[0.893 0.927]	[0.594 0.625]	[0.291 0.309]	8_{10}^2	$8_{10}^{2\ *}{+}{+}$	0	$\Sigma_{4,2}$
8_{11}^2	[4.944 4.98]	[4.423 4.455]	[0.512 0.534]	8_{11}^2	$8_{11}^{2\ *}{+}{+}$	2	$\Sigma_{2,1}$
8_{12}^2	[1.904 1.932]	[2.422 2.447]	[−0.526 − 0.508]	$8_{12}^{2\ *}$	$8_{12}^2{+}{+}$	0	$\Sigma_{4,2}$
8_{13}^2	[1.945 2.0]	[1.917 1.965]	[0.018 0.046]	$8_{13}^{2\ *}$	$8_{13}^2{+}{+}$	0	$\Sigma_{4,2}$
8_{14}^2	[3.13 3.185]	[3.17 3.218]	[−0.051 − 0.022]	8_{14}^2	$8_{14}^{2\ *}{+}{+}$	2	$\Sigma_{2,1}$
8_{15}^2	[0.029 0.056]	[0.034 0.048]	[−0.01 0.014]	8_{15}^2	$\tau 8_{15}^{2\ *}{+}{+}$	0	$\Sigma_{4,2}$
8_{16}^2	[0.188 0.219]	[0.132 0.16]	[0.05 0.065]	8_{16}^2	$8_{16}^{2\ *}{+}{+}$	2	$\Sigma_{2,1}$

6. Numerical Methods

6.1. BFACF Simulations

We use methods adopted from *Portillo et al.* and *Brasher et al.* to procure estimates of $\mathcal{S}_n(L)$, $\mathcal{S}_n(L,1)$, and $\mathcal{S}_n(L,2)$ for 2-component links [2,3]. in particular, BFACF was run to sample conformations of the 91 prime non-split 2-component links with crossing number less than or equal to

Preprints (www.preprints.org) | NOT PEER-REVIEWED | Posted: 15 August 2018 doi:10.20944/preprints201808.0265.v1

Peer-reviewed version available at Symmetry 2018, 10, 604; doi:10.3390/sym10110604

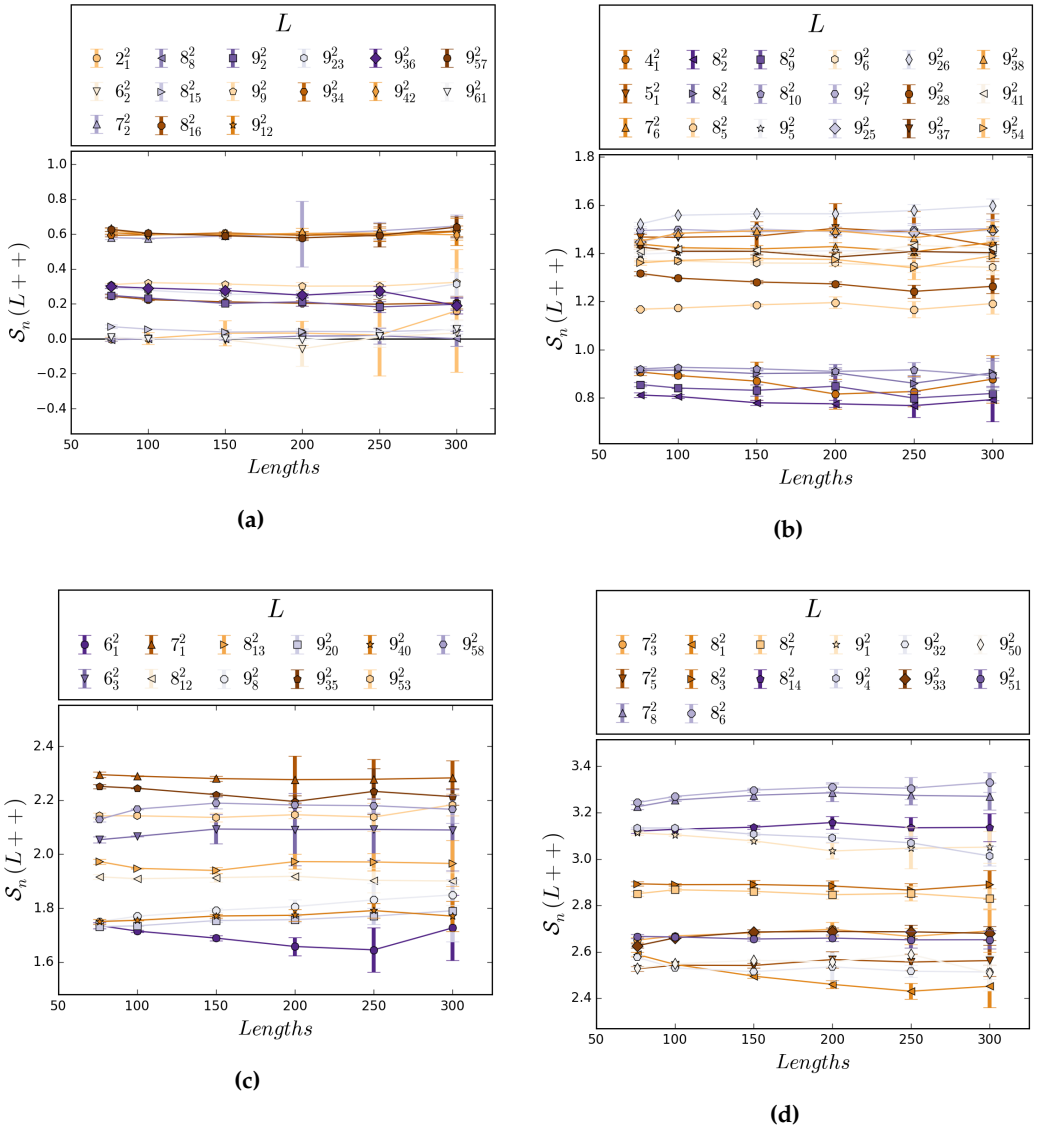

Figure 6. Graphs a-d show estimates for $\mathcal{S}_n(\mathrm{L}{+}{+})$, the average of self-writhes for links of length n and type L++, of each 2-component link with crossing number 9 or less for $n \in \{76, 100, 150, 250, \text{ and } 300\}$ as obtained from the simulations described in section 6. L++ here is the canonical link chosen as described in section 4 and listed in table A1. Only shown are links with average writhe less than 3.4, but links with larger average writhe follow similar trends. Error bars are included to indicate 95% confidence intervals. None of the error bars include 0 for links which lack reflection symmetry. The estimates do not vary widely as length increases, which demonstrates an apparent well-behaved nature of writhe for long lattice links.

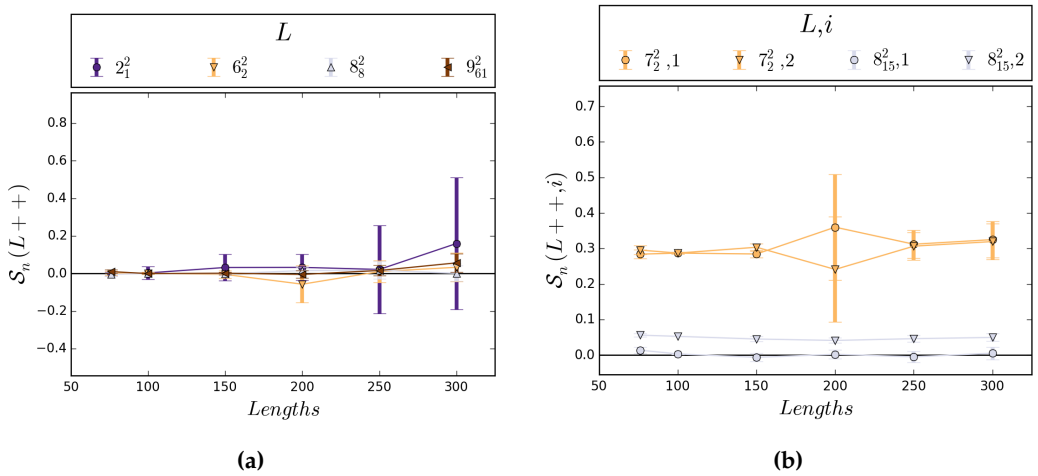

(a) **(b)**

Figure 7. (a) This graph shows 95% confidence intervals for $\mathcal{S}_n(\mathrm{L}{+}{+})$ of the four links with reflection symmetry and crossing number 9 or less for lengths 76, 100, 150, 200, 250, and 300. **(b)** This graph illustrates the expected behavior of $\mathcal{S}_n(L,i)$ for a link with pure exchange symmetry (7_2^2) and a link without pure exchange symmetry (8_{15}^2).

9. Only one isotopy class was sampled for each link, as the writhe values for other isotopy classes will be either identical or of opposite sign (as described in section 3.4). Choices of z values were chosen based on prior systematic runs used to estimate the expected length of the conformations. These same runs were also used to estimate the required number of steps between samples for statistical independence of samples. Statistical independence for these prior runs was determined by calculating integrated auto-correlation.

Samples were taken for links of length 76, 100, 150, 200, 250, and 300. Up to 20,000 independent samples were taken for most lengths of each link, with up to $2 \cdot 10^6$ and $2 \cdot 10^5$ independent samples for lengths 100 and 150, respectively. Initial sampling was done for lengths 100 and 150, but in many cases runs were terminated before all samples were taken to free up computational resources, as analysis showed the number samples already taken was more than sufficient. For the other lengths, 20,000 was selected as a sufficiently large number for the level of confidence desired. Samples were discarded and not counted if their length did not match the target length for the run.

Once the samples were obtained, the component self-writhes and the sums of self-writhes were calculated. This resulted in three lines of data for each component: the sum of self-writhes; component 1 self-writhe; and component 2 self-writhe. Batch mean analysis was then used to ensure statistical independence of these data and to calculate 95% confidence intervals for the mean of each of these values [23]. Batch mean analysis is a method which, in short, puts sequential data into blocks, if necessary, to reduce auto-correlation and uses the average of each block as a data point.

Before fully analyzing the results, we double-checked the robustness of the sampling methods by comparing certain results to known facts. First, every link with reflection symmetry must have a mean sum of self-writhes which is exactly zero. Hence, the confidence interval for $\mathcal{S}_n(L)$ must contain zero for these links. This was true of each link with symmetry group $\Sigma_{8,2}$ and $\Sigma_{4,5}$ that we sampled, and can be seen in figure 7a.

Also, for each link with the pure exchange symmetry, the mean self-writhes of each component must be exactly equal, i.e. $\mathcal{S}_n(L,1) = \mathcal{S}_n(L,2)$. To check for this, we made sure the confidence intervals for $\mathcal{S}_n(L,1)$ and $\mathcal{S}_n(L,2)$ had non-empty intersection for links with symmetry group $\Sigma_{4,1}$, $\Sigma_{8,1}$, or $\Sigma_{8,2}$ (see figure 7b). The samples taken for links with these symmetries matched our expectations as well. So, the methods appear to have sampled satisfactorily.

We did, however, require extra samples for the 8_{15}^2 link at lengths 200, 250, and 300. Since 8_{15}^2 lacks pure exchange symmetry, it is expected that $\mathcal{S}_n(L,1) \neq \mathcal{S}_n(L,2)$. The data showed this for lengths 76, 100, and 150. However, as length of a link increases, the variance of writhe also increases, which means more samples are required to maintain the same width of confidence intervals as for smaller lengths. For the 8_{15}^2 link, the self-writhes of the components are both relatively small and close together, which means they must have particularly tight confidence intervals to ensure they are disjoint. For lengths 200, 250, and 300, the confidence intervals for the self-writhe of each component were not disjoint in the original sampling of 8_{15}^2, which meant uncertainty as to whether they were distinct or if one was larger than the other. Extra samples were taken for these lengths, and with about 45000 total samples at each length, the intervals were found to be disjoint for lengths 200 and above, matching the data for lower lengths.

The Hopf link, 2_1^2 provided another issue, in that it is difficult to sample efficiently. Analysis of the autocorrelation of writhe and length of the Hopf link under BFACF moves shows that many more steps may be required between samples. Also, a high variance of length appears to cause many samples to be rejected. Because of this, the data for 2_1^2 is somewhat sparse. However, 2_1^2 has even operations symmetry with pure exchange, which means there are only 2 isotopy classes. Since the linking number of these classes are 1 and -1, we choose $2_1^2{+}{+}$ such that $\mathrm{lk}(2_1^2{+}{+}) = 1$. It is also worth noting that due to the symmetry of 2_1^2, it is necessary that $\mathcal{S}_n(2_1^2) = \mathcal{S}_{n,1}(2_1^2) = \mathcal{S}_{n,2}(2_1^2) = 0$, so sampling here serves only to test the robustness of our methods as described above.

The unlink, 0_1^2, was not sampled, as BFACF fails to converge for split links without extra restrictions such as confinement. The unlink has full symmetry, however, so there is only one choice for isotopy class and every unlink is the canonical unlink. The complete set of confidence intervals for $\mathcal{S}_n(L)$, $\mathcal{S}_n(L,1)$, and $\mathcal{S}_n(L,2)$ for all 2-component links with 9 or less crossings can be found in supplementary tables S2, S3, and S4.

6.2. Minimum Length Links

In addition to these BFACF simulations, results were obtained for minimum length lattice links from preliminary data produced by *Freund et al.* [22]. The data obtained were the set of all known minimum length conformations of each 2-component link with crossing number 9 or less. We took the assumption that these sets of conformations were complete, and calculated the mean self-writhes of the minimum lengths directly. We use the notation $\mathcal{S}_{\min}(L)$, $\mathcal{S}_{\min}(L,1)$, and $\mathcal{S}_{\min}(L,2)$ to refer to the mean self-writhes of the minimum length lattice links and their components. We took only the set of conformations representing $L{+}{+}$, as determined by our results, for each link. The results through 8 crossings are presented in table 3, and the results through 9 crossings can be found in the supplementary materials in table S1.

Supplementary Materials: The following are available online at http://www.mdpi.com/2073-8994/xx//x/, Table S1: table of mean self-writhes for minimum length lattice links extended from table 3, Table S2: table of $\mathcal{S}_n(L{+}{+})$ for all sampled n, Table S3: table of $\mathcal{S}_n(L{+}{+},1)$ for all sampled n, Table S4: table of $\mathcal{S}_n(L{+}{+},2)$ for all sampled n, Table S5: summary of link information extended from table 2, Table S6: table of canonical knot diagrams extended from the table presented by *Brasher et al.* [3].

Author Contributions: Conceptualization, S.W. and M.V.; Methodology, S.W., M.F. and M.V. ; Software, S.W. and M.F.; Validation, S.W., M.F. and M.V.; Formal Analysis, S.W., M.F. and M.V.; Investigation, S.W. and M.F.; Resources, M.V.; Data Curation, M.F. and S.W.; Writing – Original Draft Preparation, S.W., M.F. and M.V.; Writing – Review & Editing, S.W., M.F. and M.V.; Visualization, S.W., M.F. and M.V.; Supervision, M.V..; Project Administration, M.V.; Funding Acquisition, M.V.

Acknowledgments: This research was supported with the National Science Foundation CAREER Grant DMS1519375 and DMS1716987 (MF, MV, SW). The authors are grateful to the following individuals: R. Scharein for providing assistance with Knotplot; R. Stolz for assistance with batch mean analysis; R. Brasher for assistance with BFACF; Priya Kshirsagar for preliminary work. We are indebted to Chris Soteros, Koya Shimokawa, and to Javier Arsuaga and other members of the Arsuaga-Vazquez lab for valuable feedback.

Conflicts of Interest: The authors declare no conflict of interest.

Appendix A Link Table

Table A1. Regular oriented diagrams representing the canonical link isotopy classes L++ as described in section 4. Next to each link name is its symmetry group, which may be cross-referenced with table 1. For links lacking pure exchange symmetry, the lighter blue strand is labeled as component 1 and the darker red-orange strand is component 2.

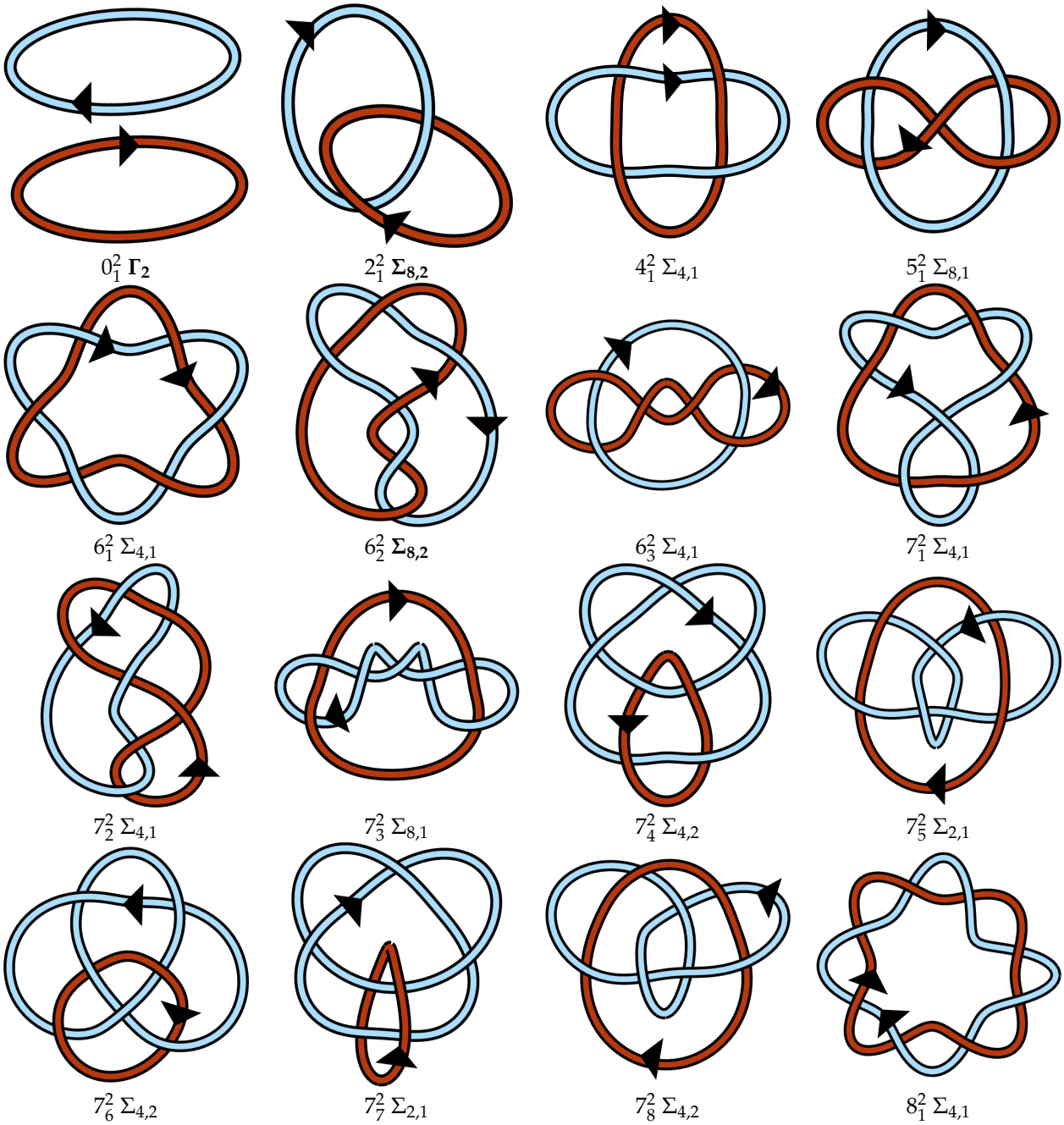

Peer-reviewed version available at Symmetry 2018, 10, 604; doi:10.3390/sym10110604

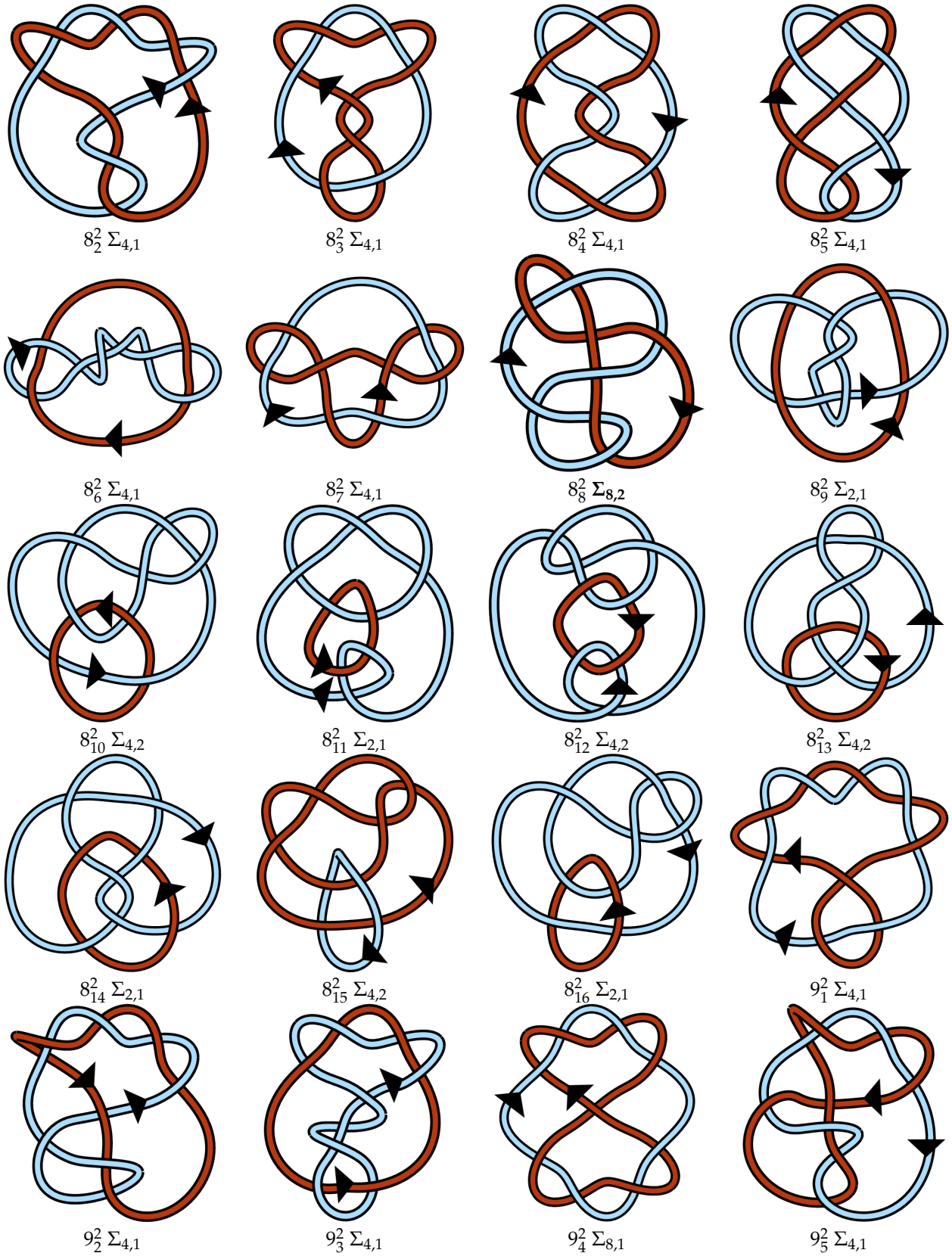

Peer-reviewed version available at Symmetry 2018, 10, 604; doi:10.3390/sym10110604

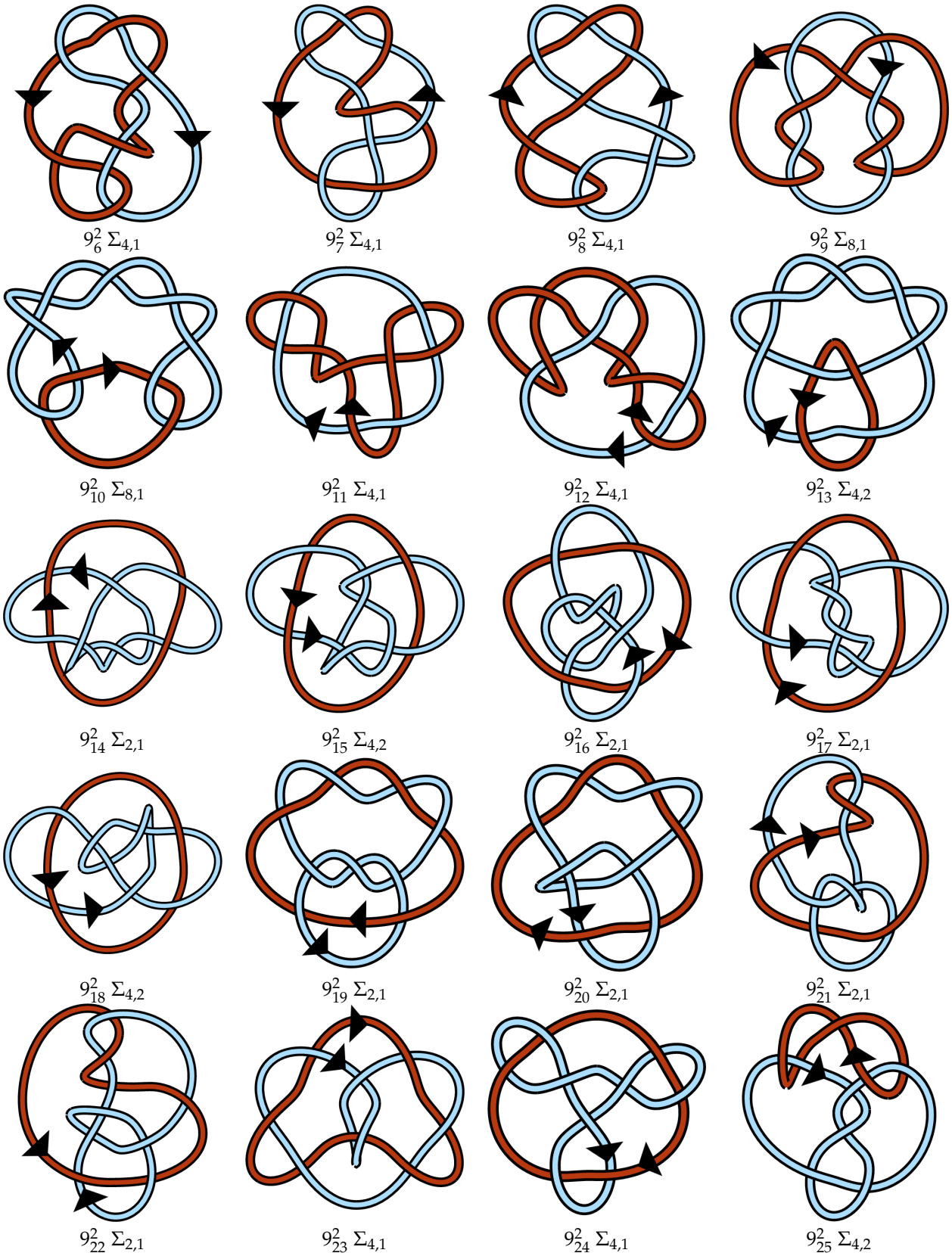

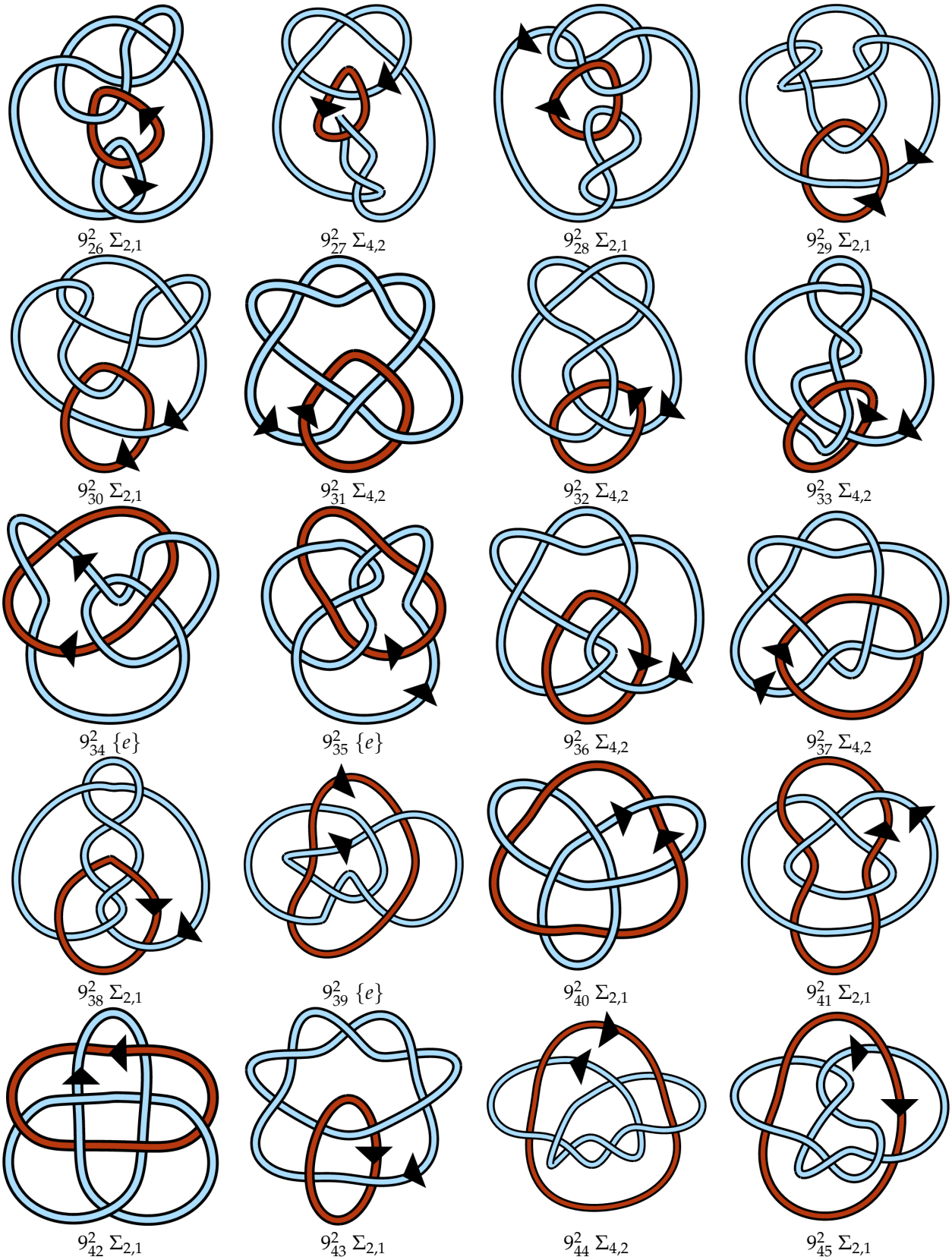

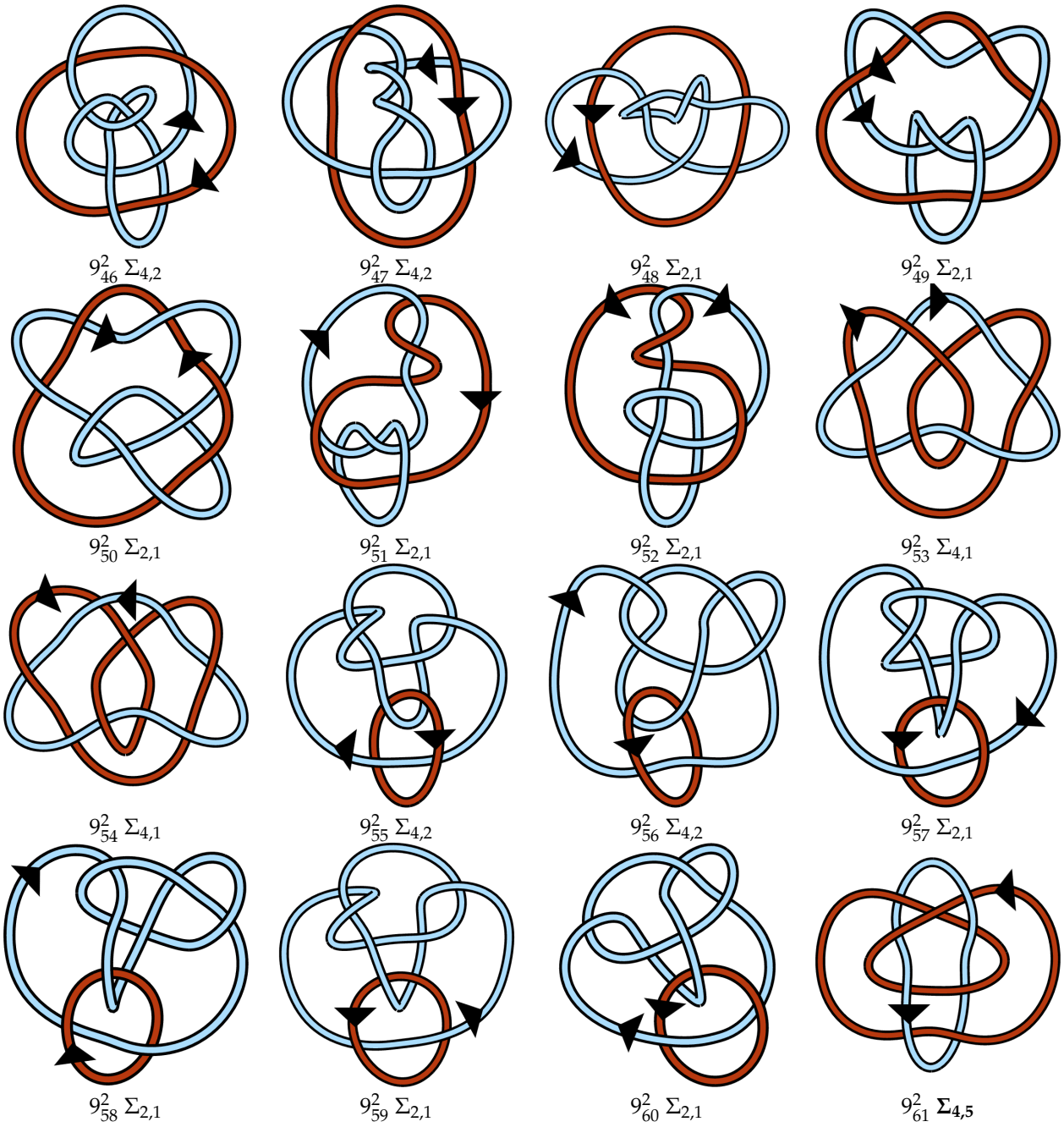

References

1. Rolfsen, D. *Knots and Links*; AMS/Chelsea Publication Series, AMS Chelsea Pub., 1976.
2. Portillo, J.; Diao, Y.; Scharein, R.; Arsuaga, J.; Vazquez, M. On the mean and variance of the writhe of random polygons. *J Phys A Math Theor* **2011**, *44*, 275004. doi:10.1088/1751-8113/44/27/275004.
3. Brasher, R.; Scharein, R.G.; Vazquez, M. New biologically motivated knot table. *Biochem Soc Trans* **2013**, *41*, 606–611. doi:10.1042/BST20120278.
4. Grainge, I.; Bregu, M.; Vazquez, M.; Sivanathan, V.; Ip, S.C.; Sherratt, D.J. Unlinking chromosome catenanes in vivo by site-specific recombination. *The EMBO journal* **2007**, *26*, 4228–4238.
5. Shimokawa, K.; Ishihara, K.; Grainge, I.; Sherratt, D.J.; Vazquez, M. FtsK-dependent XerCD-dif recombination unlinks replication catenanes in a stepwise manner. *Proceedings of the National Academy of Sciences of the United States of America* **2013**, *110*, 20906–11. doi:10.1073/pnas.1308450110.

6. Stolz, R.; Yoshida, M.; Brasher, R.; Flanner, M.; Ishihara, K.; Sherratt, D.J.; Shimokawa, K.; Vazquez, M. Pathways of DNA unlinking: A story of stepwise simplification. *Scientific Reports* **2017**, *7*, 12420. doi:10.1038/s41598-017-12172-2.
7. Klenin, K.; Langowski, J. Computation of writhe in modeling of supercoiled DNA. *Biopolymers* **2000**, *54*, 307–317. doi:10.1002/1097-0282(20001015)54:5<307::AID-BIP20>3.0.CO;2-Y.
8. Berglund, M.; Cantarella, J.; Casey, M.P.; Dannenberg, E.; George, W.; Johnson, A.; Kelley, A.; LaPointe, A.; Mastin, M.; Parsley, J.; Rooney, J.; Whitaker, R. Intrinsic Symmetry Groups of Links with 8 and Fewer Crossings. *Symmetry* **2012**, *4*, 143–207, [1010.3234]. doi:10.3390/sym4010143.
9. Doll, H.; Hoste, J. A tabulation of oriented links. *Math. Comp.* **1991**, *57*, 747–761. With microfiche supplement, doi:10.2307/2938715.
10. Cantarella, J.; Cornish, J.; Mastin, M.; Parsley, J. The 27 Possible Intrinsic Symmetry Groups of Two-Component Links. *Symmetry* **2012**, *4*, 129–142. doi:10.3390/sym4010129.
11. Henry, S.R.; Weeks, J.R. Symmetry Groups of Hyperbolic Knots and Links. *Journal of Knot Theory and Its Ramifications* **1992**, *01*, 185–201. doi:10.1142/S0218216592000100.
12. Liang, C.; Cerf, C.; Mislow, K. Specification of chirality for links and knots. *Journal of Mathematical Chemistry* **1996**, *19*, 241–263. doi:10.1007/BF01166717.
13. Berg, B.; Foerster, D. Random paths and random surfaces on a digital computer. *Physics Letters B* **1981**, *106*, 323–326.
14. De Carvalho, C.A.; Caracciolo, S. A new Monte-Carlo approach to the critical properties of self-avoiding random walks. *Journal de Physique* **1983**, *44*, 323–331.
15. De Carvalho, C.A.; Caracciolo, S.; Fröhlich, J. Polymers and g$|\varphi|$4 theory in four dimensions. *Nuclear Physics B* **1983**, *215*, 209–248.
16. Van Rensburg, E.J.; Whittington, S. The BFACF algorithm and knotted polygons. *Journal of Physics A: Mathematical and General* **1991**, *24*, 5553.
17. Madras, N.; Slade, G. *The self-avoiding walk*; Probability and its applications, Birkhäuser, 1993.
18. Hypnagogic Software. KnotPlot. http://www.knotplot.com/ (10/24/2014).
19. Laing, C.; Sumners, D.W. Computing the writhe on lattices. *Journal of Physics A: Mathematical and General* **2006**, *39*, 3535–3543. doi:10.1088/0305-4470/39/14/003.
20. Lacher, R.; Sumners, D. Data structures and algorithms for computation of topological invariants of entanglements: link, twist and writhe, 1991.
21. Culler, M.; Dunfield, N.M.; Goerner, M.; Weeks, J.R. SnapPy, a computer program for studying the geometry and topology of 3-manifolds. http://snappy.computop.org (03/13/2017).
22. Freund, G.; Witte, S.; Vazquez, M. Bounds for the Minimum Step Number for 2-Component Links in the Simple Cubic Lattice. In progress.
23. Fishman, G. *Monte Carlo: Concepts, Algorithms, and Applications*; Springer Series in Operations Research and Financial Engineering, Springer New York, 2013.